Journal of Alloys and Compounds 861 (2021) 158534

Contents lists available at ScienceDirect

Journal of Alloys and Compounds

journal homepage: www.elsevier.com/locate/jalcom

Long-term-stable WO_3-PB complementary electrochromic devices

Kun Wang[a,c], Hongliang Zhang[a,*], Guoxin Chen[a], Tian Tian[a], Kai Tao[c], Lingyan Liang[a], Junhua Gao[a], Hongtao Cao[a,b,**]

[a] Laboratory of Advanced Nano Materials and Devices, Ningbo Institute of Materials Technology and Engineering, Chinese Academy of Sciences, Ningbo 315201, People's Republic of China
[b] Center of Materials Science and Optoelectronics Engineering, University of Chinese Academy of Sciences, Beijing 100049, People's Republic of China
[c] Institute of Inorganic Materials, School of Materials Science and Chemical Engineering, Ningbo University, Ningbo 315211, People's Republic of China

ARTICLE INFO

Article history:
Received 5 November 2020
Received in revised form 23 December 2020
Accepted 27 December 2020
Available online 29 December 2020

Keywords:
Electrochromic devices
Tungsten oxide
Prussian blue
Synergistic effects
Active interface

ABSTRACT

The complementary electrochromic devices based on WO_3 and Prussian blue electrodes (PB) have shown a limited chemical stability and durability because WO_3 is degraded in electrochromic performance and PB is gradually dissolved in the Li^+-based electrolyte under neutral pH conditions. Herein, the utilization of acetic acid as super-additive solution was proposed to improve WO_3 cathodes and stabilize PB anodes, in which the highly nanoporous nanocrystal-in-glass WO_3 and hierarchical PB was made by electron beam evaporation and electrochemical deposition method, respectively. Our findings suggest that synergistic effects of Li^+ and H^+ on WO_3 and Prussian blue electrodes contribute to the improvement on electrochemical, electrochromic, and cycling stability performance of the whole device. Impressively, the WO_3-PB complementary electrochromic device could experience a superior long-term cycling stability of over 10,000 cycles, with a high coloration efficiency of 137.80 cm^2 C^{-1} and a maximum transmittance modulation of 66.22%@ 633 nm. All these results open a new way to the construction of high-performance electrochromic devices.

1. Introduction

The certain electroactive materials, which reversibly change their colors or optical properties (absorbance/transmittance/reflectance) via redox reactions under an external voltage or current, are called electrochromic materials [1,2]. Electrochromic devices (ECDs) composed of these materials have received considerable attention in recent years because of their potential applications such as smart windows [3], displays [4,5] and rear-view mirrors [6]. A complementary electrochromic device is made of both anodic and cathodic electrochromic materials that can be darkened or bleached in phase, yielding desirable electrochromic performance such as fast coloration, high optical modulation, high coloration efficiency, good cyclic stability and low energy consumption due to charge matching, redox balance, and so on [7–12]. The inorganic electrochromic materials can be categorized into two major classes, namely, transition metal oxides (TMOs) and Prussian blue (PB)-based systems [13]. Tungsten oxide (WO_3), as one of the most attractive cathodic electrochromic materials in TMOs, has fascinating EC properties such as high cyclic stability and coloration efficiency [14,15]. It is well known that H^+ or Li^+-based electrolyte is anticipated to be a high performance electrolyte material in the WO_3-based electrochromic devices due to the small ion radius [16]. So far, the WO_3-based electrochromic devices are still far from the desired cycle life for practical applications [17–19]. One of the reasons is the limited reversibility of Li^+ in the amorphous WO_3 [20–22]. Even WO_3 is still slightly soluble in sulfuric acid electrolytes at room temperature [23]. In addition, another critical factor in limiting the cycle life of WO_3 electrodes is the formation of an unstable counter electrodes at the active interface between counter electrodes and electrolytes, which becomes especially crucial in double injection/extraction of ions/electrons in response to the applying voltages. Prussian blue (PB), $[Fe^{3+}Fe^{2+}(CN)_6]^-$, and its nanocomposites have been proven to be one of the most promising candidates as the electrochromic anode in K^+-based electrolyte [24]. For instance, the electrochemically deposited PB thin films in K^+-based electrolyte have demonstrated a good performance with a high electrochromic contrast of 55.36% at 555 nm and sound stability [25]. However, K^+ usually shows relatively slow diffusion kinetics due to its large radii [26]. Very recently,

* Corresponding author.
** Corresponding author at: Laboratory of Advanced Nano Materials and Devices, Ningbo Institute of Materials Technology and Engineering, Chinese Academy of Sciences, Ningbo 315201, People's Republic of China.
E-mail addresses: zhanghl@nimte.ac.cn (H. Zhang), h_cao@nimte.ac.cn (H. Cao).

https://doi.org/10.1016/j.jallcom.2020.158534
0925-8388/

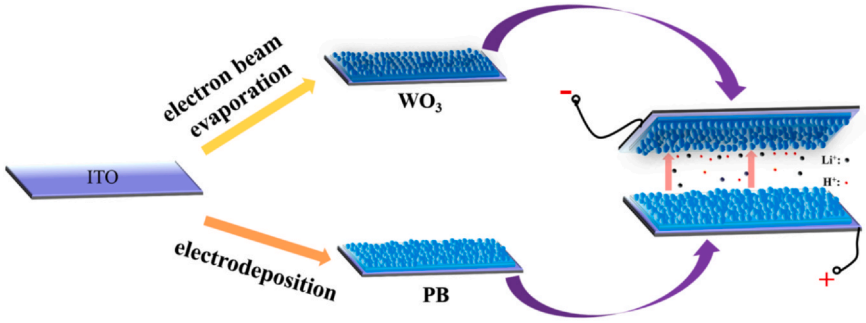

Fig. 1. Schematic illustration of the process of preparing the WO_3-PB complementary ECD.

the electrochromic device based on hexagonal WO_3 and NiO/PB composite nanosheet electrodes shows the ability to insert / extract the lithium ions reversibly and good cyclic stability about 4000 cycles [27]. Impressively, the introduction of acetic acid to the PC-$LiClO_4$ electrolyte can improve the stability of the PB thin films [28]. The application of WO_3 and PB electrodes in the field of electrochromism and electrochemistry has proliferated in recent years, however, the long-term-stable complementary electrochromic device based on the two excellent materials, especially in lithium ion electrolyte with proton, is lacking.

Herein, the effect of acetic acid on electrochemical and electrochromic performance of the electron beam evaporated WO_3 thin films and electrochemically deposited PB films in PC-$LiClO_4$ electrolyte is investigated. The fabrication process of the complementary electrochromic devices based on WO_3 and PB electrodes is depicted in Fig. 1. The WO_3-PB complementary electrochromic devices manifest a high performance with a superior cyclic stability over 10,000 switching cycles.

2. Experimental

2.1. Materials

All chemicals were of analytical grade. Potassium ferricyanide ($K_3Fe(CN)_6$, ≥99.5%), potassium chloride (KCl, ≥99.5%) and hydrochloric acid (HCl, 36%–38%) were obtained from Sinopharm Chemical Reagent Co.Ltd. Iron chloride hexahydrate ($FeCl_3.6\,H_2O$, AR, 99%) and acetic acid ($C_2H_4O_2$, ≥99.8%) were purchased from Aladdin. Both the electrochemically deposited PB films and the e beam evaporated WO_3 thin films were deposited on the conducting transparent indium tin oxide (ITO)-coated glass substrates with the sheet resistance of 10 Ohm/sq.

2.2. Preparation of the WO_3 thin films

The WO_3 thin films were deposited on the ITO-coated glass at the substrate temperatures of 200 °C by an electron beam evaporation technique (MUE-ECO made in ULVAC, Japan). The background pressure was reduced to less than 2×10^{-3} Pa. Several pure WO_3 particles with the diameter of ~3 mm in a tungsten crucible were bombarded by an electron beam of 10 kV. The deposition rate and the thickness of thin films were 0.10–0.20 nm/s and approximately 300 nm, respectively.

2.3. Preparation of the PB films

Electrochemical deposition was conducted in a conventional three electrode cell including glass/ITO, SCE, and Pt plate as working, reference and counter electrodes. The PB films were electrochemically deposited from a solution containing 10 mM $FeCl_3.6\,H_2O$, 10 mM $K_3Fe(CN)_6$, 0.10 M KCl and 0.10 M HCl. A constant cathodic current density of 20 mA cm^{-2} was applied to the ITO substrates in the electrochemical workstation for 5 mins. The as-deposited PB films were washed with ethanol and deionized water to remove the excess of solution. Finally, all the PB films were dried at 60 °C in air for 6 h and stored in air for the further experiments.

2.4. Assembly of the devices

The typical devices were constructed by sandwiching a Li^+ electrolyte with acetic acid between the electron beam evaporated WO_3 thin film on the ITO-coated glass and a counter electrode which was also ITO glass coated by electrochemically deposited PB film. The complementary ECDs with ITO/WO_3/electrolyte/PB/ITO configuration were assembled by injecting 0.10 M PC-$LiClO_4$ electrolytes with 0.01 M acetic acid as the electrolyte into the spacing between two electrodes in the vacuum filling process, similar to the previous report [29].

2.5. Measurements

The structure and morphology of the WO_3 thin films and PB films were analyzed by X-ray diffraction (XRD, Bruker D8 Advance using Cu-Kα (λ = 0.154178 nm) radiation and a θ-2θ configuration) and thermal field-emission scanning electron microscopy (TFESEM; Verios G4 UC, Thermo Scientific, USA). The spectroscopic test apparatus in conjunction with a UV–VIS–IR spectroscopy (PerkinElmer Lambda 950) and an electrochemical workstation (CHI660D, Chen hua Shanghai) was employed to measure optical transmittance spectra of the films in the three-electrode system and the electrochromic devices in the two-electrode system. The time-dependent optical transmittance spectra of the films were acquired, under applied voltage by an electrochemical workstation, by placing the film as working electrode in a liquid spectroelectrochemical cell. Electrochemical measurements of films were carried out in a three-electrode cell. A platinum sheet and KCl saturated $Hg/HgCl_2$ were used as counter electrode and reference electrode, respectively. 0.10 M $LiClO_4$-PC electrolytes without and with 0.01 M acetic acid were used as the electrolyte. Electrochemical measurements of the complementary ECDs with 0.01 M acetic acid as the electrolyte were carried out in the two-electrode system. The chronoamperometry, chronocoulometry and cyclic voltammetry measurements were conducted by applying voltage between −1.00 V and + 1.00 V for the WO_3 thin films, between −0.80 V and +1.00 V for the PB films, between −1.50 V and + 1.60 V for ECDs respectively. The electrochemical impedance spectra were measured on an electrochemical workstation (Zennium, IM6) in the frequency range from 100 mHz to 100 kHz.

3. Results and discussion

3.1. Electrochromic performance of the WO_3-PB complementary devices

The wavelength-dependent optical transmittance spectra and digital photos (inset) of the complementary ECDs based on WO_3 and

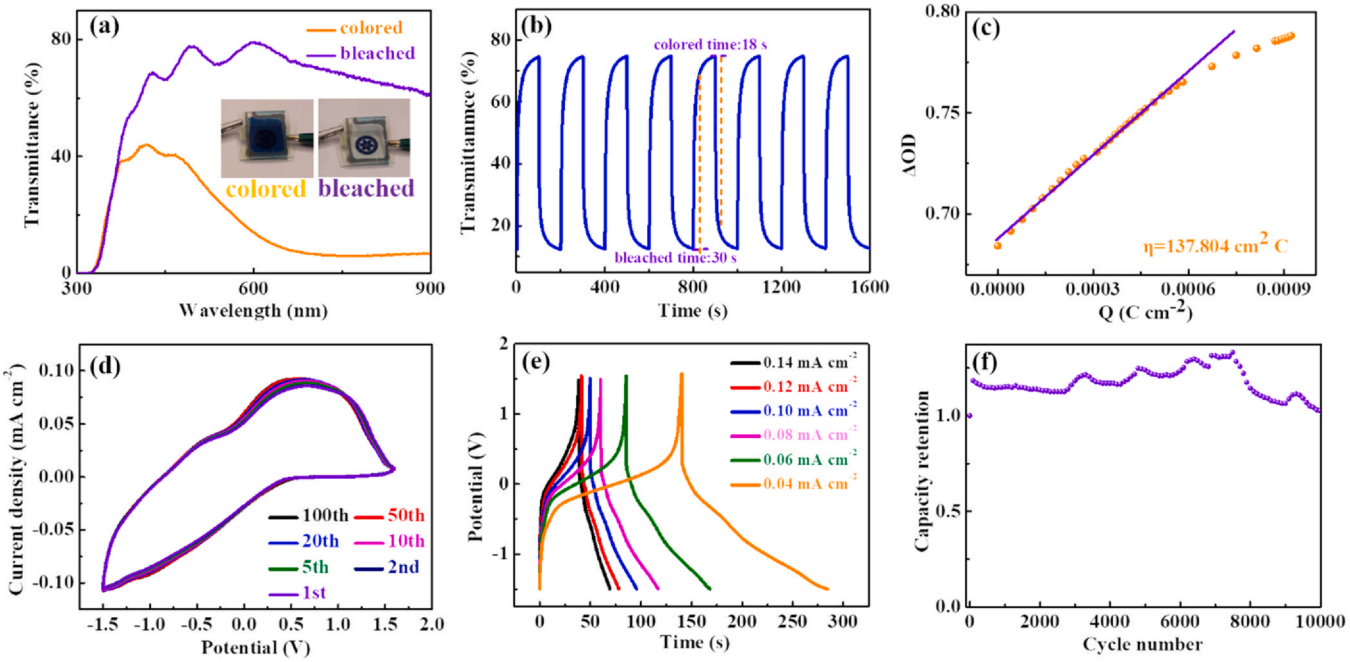

Fig. 2. (a) The wavelength-dependent optical transmittance spectra, photographs (inset), (b) the time-dependent optical transmittance spectra at $\lambda_{633\,nm}$ (−1.5 V/+1.6 V, 200 s per cycle), (c) plots of the time-dependent optical density variation as a function of charge density at $\lambda_{633\,nm}$, (d) cyclic voltammograms (CVs) at the scan rate of 50 mV/s, (e) GCD curves at various current densities, and (f) cyclic performance at a current density of 0.12 mA cm^{-2} for the complementary WO_3-PB ECD.

Prussian blue electrodes in the bleached state of +1.60 V and colored state of −1.50 V are shown in Fig. 2(a). The transmittance modulation (ΔT), described as the transmittance difference between the bleached and colored states at a certain wavelength, is calculated to be 66.22% (633 nm), comparable to the previous report (67.6%, in the WO_3-NiO/PB ECD) [27]. The WO_3-PB complementary ECD is dark blue in the colored state and becomes transparent in its bleached one, as manifested in the inset of Fig. 2(a). Figs. 2(b) and S7d respectively displays the time-dependent transmittance spectra and the charge density response for the complementary ECDs at 633 nm obtained by alternately applying a −1.50 V and + 1.60 V voltage both for 100 s. The coloring and bleaching response time, which is defined as the time required to reach 90% of the transmittance change between bleached and colored state, is calculated to be 18 s and 30 s, respectively. It benefits from the configuration of the complementary ECDs [30,31]. The injection/extraction of ions (Li^+ and H^+) and electrons into/from the WO_3 electrode is accompanied by the extraction/injection of ions and electrons from/into the PB counter electrode. Coloration efficiency, another key criteria for the EC devices, is calculated to be 137.80 cm^2 C^{-1} (Fig. 2(c)), larger than the reported value of 25.90 cm^2 C^{-1} [32] and 60.20 cm^2 C^{-1} [33] in WO_3-based ECDs. A high coloration efficiency indicates that the device is capable of possessing large optical modulation with a small charge variation [34], in favor of long-term cyclic stability because of released charge accumulation and extraction stress [35]. The electroactivity reflected by the encapsulated area of the CV curve in the potential region from −1.50–1.60 V with a scan rate of 50 mV/s is even improved after 100 cycles (Fig. 2(d)), suggesting a good electrochemical stability of the device, as reported previously [36]. A series of relatively symmetrical galvanostatic charge/discharge curves at various current densities from 0.04 mA cm^{-2} to 0.14 mA cm^{-2} are shown in Fig. 2(e), indicating a reversible redox reaction [37]. It is generally believed that the cyclic retention is a major concern in the practical application of ECDs. Our device has an outstanding long-term cycle stability with a capacitance retention of 102.62% after 10,000 continuous cycles (for 10 days) under the current density of 0.12 mA cm^{-2}, as displayed in Fig. 2(f). In particular, the capacitance retention was increased slightly after dozens of initial cycles, owing to the fact that the WO_3 and PB electrodes were modified by the Li^+-based electrolyte with acetic acid involved on one hand, and the specific capacitance was magnified as increasing the effective specific surface area on the other [38]. To analyze the origin of long-term cyclic stability of WO_3-PB complementary ECDs, the electrochemical and electrochromic performance of active interfaces of WO_3/electrolyte and PB/electrolyte will be discussed as follows.

3.2. Electrochemical properties

In order to inhibit the decomposition of the PB films and improve the electrochromic performance of the WO_3 thin films in PC-$LiClO_4$ electrolyte, 0.01 M acetic acid is added to the electrolyte (pH=2.06), in hope of improving the stability of the films during double injection / extraction of electrons and ions [28].

3.2.1. Electrochemical properties of the WO_3 thin films

The cyclic voltammetry curves determined by the electrochemical measurements at different scan rate from 10 mV/s to 100 mV/s between −1.00 V and + 1.00 V in the three-electrode system are shown in Figs. 3a and S3. It can be seen that the peak values of the current density of the WO_3 thin films in PC-$LiClO_4$ electrolyte without and with acetic acid are increased accordingly with the scan rate. There is no obvious difference for the peak current density between at 90 mV/s and 100 mV/s, probably due to the saturation of the ion diffusion. In addition, the cyclic voltammetry curves are similar for the WO_3 thin films in PC-$LiClO_4$ electrolyte with or without acetic acid at the same scan rate. The charge density variations to reveal the color change process are obtained via the chronocoulometry method by supplying a square-wave voltage of −1.00 V and + 1.00 V with a pulse width of 45 s (Fig. 3b). The maximum charge density is determined to be about −48.18 and −37.70 mC cm^{-2} for the WO_3 thin films in the Li^+-based electrolyte with and without acetic acid, respectively, suggesting the charge capacity improvement with the addition of acetic acid. To further investigate the ion diffusion mechanism, the relationship

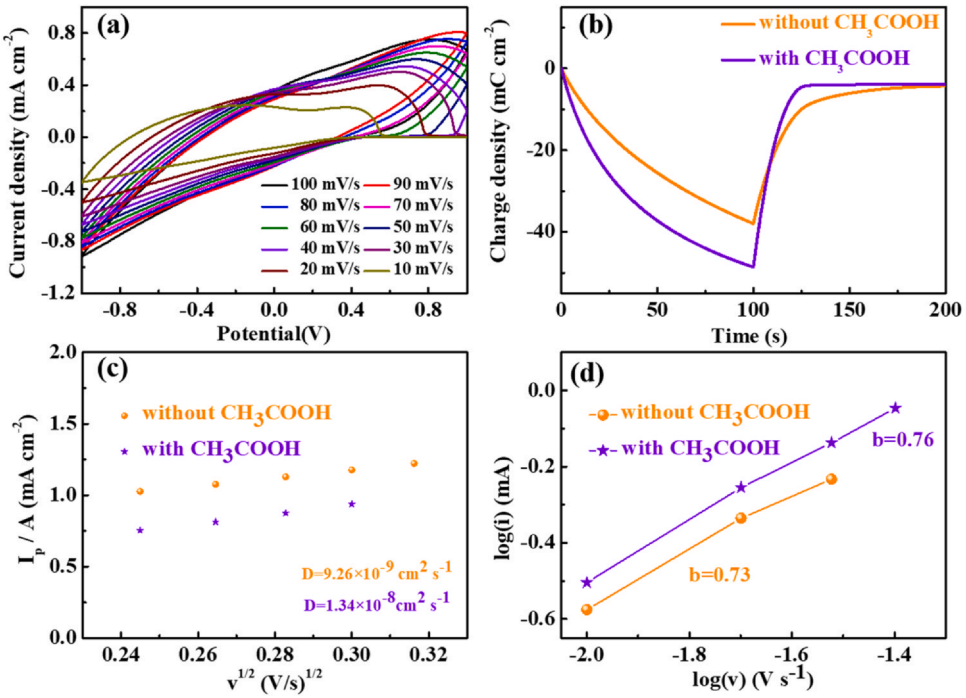

Fig. 3. (a) Cyclic voltammograms (CVs) of the WO_3 film in PC-$LiClO_4$ electrolyte with acetic acid at the scan rates of 10, 20, 30, 40, 50, 60, 70, 80, 90 and 100 mV/s, respectively. (b) Charge density, (c) dependence of the peak current densities (I_p) versus the square root of scan rate ($v^{1/2}$) and (d) power law dependence of the peak current versus the scan rate for the WO_3 thin films in PC-$LiClO_4$ electrolyte with and without acetic acid.

between the peak current (i) and scan rate (v) is obtained. As illustrated in Fig. 3(c), the diffusion coefficient (D) for the WO_3 thin films in the Li^+-based electrolyte without and with acetic acid is 9.26×10^{-9} and 1.34×10^{-8} cm^2 s^{-1}, respectively, both larger than the value (1.29×10^{-10} cm^2 s^{-1}) in the previous report [39]. Large diffusion coefficient is in favor of fast switching response, as stated previously [40]. On the one hand, the larger diffusion coefficient could be due to nanocrystal-in-glass and highly nanoporous structures of the WO_3 thin films (Fig. S2 in the Supporting Information), which facilitate ion conduction. On the other hand, generally speaking, the diffusion coefficient is closely related to: (1) the radii of solvated species, and (2) the feature of the ionic charge [41]. It is conceivable that the synergistic diffusion of Li^+ and H^+ accounts for the large diffusion coefficient. Moreover, the total stored charge can be separated into two components: the faradaic contribution and the non-faradaic one. These capacitive effects are characterized by analyzing the 'b′ value that is calculated by the following equation[42]:

$$i = av^b, \tag{1}$$

where the peak current (i) obeys a law power in response to the scan rate (v). Both 'a′ and 'b′ are the adjustable parameters and the 'b′ value is determined from the slope of log(i) versus log(v). It is noteworthy that the slope of ~0.5 and ~1.0 represents the dominance of semi-infinite linear diffusion and the surface-controlled (capacitive) electrochemical reaction, respectively [43]. As revealed in Fig. 3(d), the 'b′ value of the WO_3 thin films in the Li^+-based electrolyte without and with acetic acid is calculated respectively to be 0.73 and 0.76 (in between 0.5 and 1), suggesting that the charge storage is a combination of semi-infinite diffusion and capacitive reactions.

3.2.2. Electrochemical properties of the PB films

In order to understand the electrochemical behavior of the PB films in the Li^+-based electrolyte with acetic acid, the CV curves were measured at different scan rates ranging from 10 mV/s to 100 mV/s between −0.80 V and +1.00 V in the traditional three-electrode system (Fig. 4a). It can be seen that there is a pair of distinct redox peaks whose value is increased with scan rate. Further, the relationship between the peak current (i) and scan rate (v) is plotted in Fig. 4b to investigate the ion diffusion behaviors. It is apparent that there is a favorable linear relationship between peak current and the square root of scan rate. The diffusion coefficient derived from the corresponding slope is 2.06×10^{-8} cm^2 s^{-1}, larger than the corresponding values (10^{-9} - 10^{-10} cm^2 s^{-1}) in the K^+-based electrolyte [44]. Actually, the hierarchical structure of the PB film could account for the large diffusion coefficient (Fig. S2 in the Supporting Information). Similarly, the 'b′ value of the PB films is estimated to be 0.77 (Fig. 4c), also revealing that the current is limited by both semi-infinite linear diffusion and capacitive-controlled one. The capacitive contributed charge Q_c, which helps to deeply analyze the charge storage kinetics of the PB films, is derived from the following equation[45]:

$$Q(v) = Q_c + k \times v^{-1/2}, \tag{2}$$

where k is a constant and $k \times v^{-1/2}$ represents the diffusion-controlled charge. The Q_c can be obtained from the total charge (Q, mC cm^{-2}) versus $v^{-1/2}$ (scan rate, mV s^{-1}) plots. According to Fig. S4, Q_c is calculated to be approximately 12.03 mC cm^{-2} when the scan rate reaches infinite. On the basis of the calculated Q_c, the ratios of capacitive-controlled and the diffusion-controlled contribution to the total charge at different scan rates are depicted in Fig. 4(d). It is well known that both the capacitive-controlled and diffusion-controlled contribution are a qualitative analysis. By means of the integration of the current density over a CV curve, a relatively high capacitive charge ratio of ~ 92% at the scan rate of 90 mV/s was yielded. Also, the capacitive-controlled charge contribution is gradually increased with the scan rate. By parallel comparison, the dominance of the capacitive-controlled charge contribution is in a good agreement with the 'b′ values calculated previously.

3.3. The transmittance spectra and electrochromic properties of the films

To characterize the EC performance of the WO_3 thin films and PB films, the wavelength-dependent optical transmittance spectra in

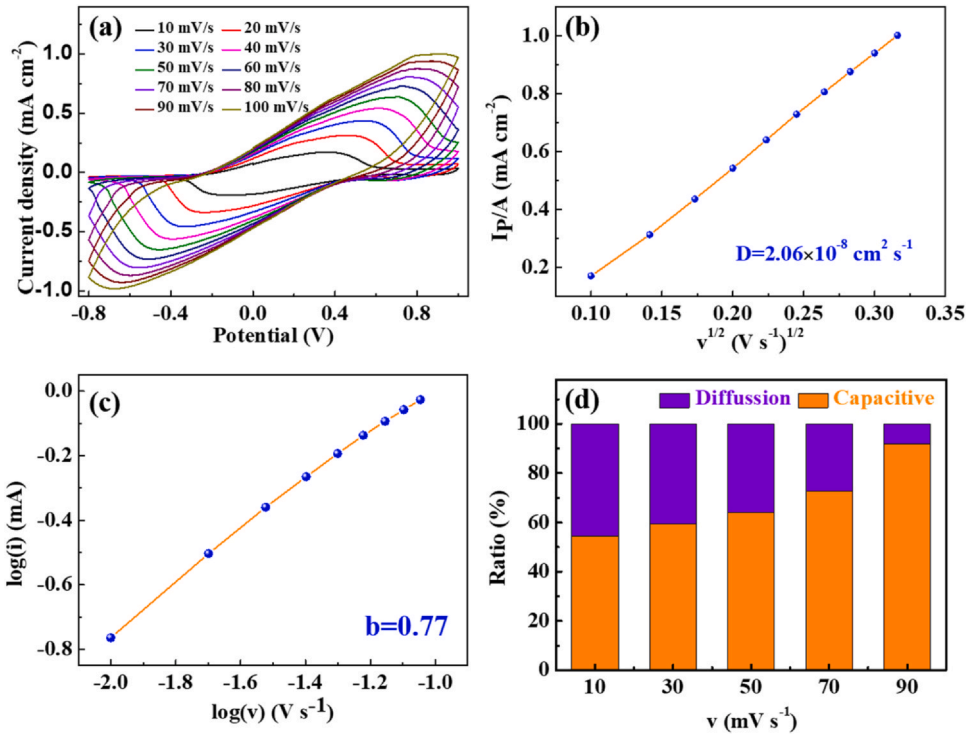

Fig. 4. (a) Cyclic voltammograms (CVs) of the PB films at different scan rates, (b) dependence of the peak current densities (I_p) versus the square root of scan rate ($v^{1/2}$) at different scan rates, (c) power law dependence of the peak current versus the scan rate, and (d) separation of contributions from capacitive- and diffusion-controlled processes as a function of processes at different scan rates for the PB films in PC-$LiClO_4$ electrolyte with acetic acid.

the wavelength range of 300–900 nm (Fig. S6a) and the time-dependent optical transmittance spectra at 633 nm were recorded. Fig. 5(a) illustrates the time-dependent optical transmittance spectra of the WO_3 thin films by alternately applying a −1.00 V/+ 1.00 V voltage for 90 s/45 s. The maximum transmittance modulation (ΔT) for the WO_3 thin films in the Li^+-based electrolyte with acetic acid is about 85.02%, higher than the value (82.48%) without acetic acid. Moreover, the optical transmittance modulation is attenuated by 14.40% after 20 cycles without using acetic acid, while it is only reduced by 3.69% with the addition of acetic acid. According to the mechanism proposed by Bohnke [46], the degradation of the WO_3 thin films can be due to the formation of Li_2WO_4, which is produced by the following reactions:

$$W\text{-}OH + Li^+ \rightarrow W\text{-}OLi + H^+$$

The formation of Li_2WO_4 will be prevented by adding an acid to the electrolyte, as reported previously [47]. Thus, it is believed that the addition of acetic acid could inhibit the degradation of the WO_3 films and increase the electrochemical reversibility in terms of the ease of injection / extraction of ions (Li^+ and H^+) / electrons, resulting in the long-term-stable electrochromic cycles. The colored / bleached response time (Fig. S6b), which is defined as the time required to reach 90% of the transmittance change between bleached and colored state[48], is estimated to be about 25 s / 30 s and 33 s / 19 s for the WO_3 thin films in the Li^+-based electrolyte without and with acetic acid, respectively. The faster bleached response time is impressive when using acetic acid. Basically, the intercalation is mostly governed by the charge transfer resistance between the electrode and electrolyte, whereas the extraction is mainly influenced by ionic transport at electrode/electrolyte active interface [49]. Thus, the shorter bleached response time may stem from the faster ionic transport (synergistic ionic transport effect of Li^+ and H^+) through active interface. What is noteworthy is that the electrochromic performance of the PB films without using acetic acid failed only after 10 cycles (Fig. S5). However, the PB film in the Li^+-based electrolyte with acetic acid presents an outstanding long-term-stable optical switching, as proved by the time-dependent optical transmittance spectra in Fig. 5(b). The critical reason is that protons at the active interface of the PB films can inhibit the formation of Fe $(OH)_2/Fe(OH)_3$ compound, causing the $[Fe^{3+}Fe^{2+}(CN)_6]^-$ complex to be maintained. Therefore, the synergistic effect of Li^+ and H^+ on PB electrode contributes to the stable optical modulation. In addition, both the coloration and bleaching time are equal to 7.0 s, which is regard as the dominant of pseudocapacitive behavior [49].

The coloration efficiency (CE), defined as the change of optical density (OD) per unit of charge density [50], can be calculated from the slope of the linear regime of the plot. Figs. 5c and Fig. S8 show the plots of optical density variation (ΔOD) at 633 nm as a function of charge density (Q) of the WO_3 thin films in the Li^+-based electrolyte with or without acetic acid, yielding the coloration efficiency (η) of 50.87 $cm^2\ C^{-1}$ and 47.48 $cm^2\ C^{-1}$, respectively. The result demonstrates that the same amount of injected charge would gain more remarkable color change with the addition of acetic acid. As displayed in Fig. 5(d), the coloration efficiency (η) of the PB films in the Li^+-based electrolyte with acetic acid is calculated to be 223.186 $cm^2\ C^{-1}$, larger than that (99.00 $cm^2\ C^{-1}$) of the PB thin films in the K^+-based electrolyte [51]. A possible reason lies in the smaller radius of H^+ and Li^+ as compared to that of K^+, then H^+ and Li^+ can be intercalated and deintercalated more easily and reversibly.

3.4. Electrochemical impedance spectra

Electrochemical impedance spectroscopy tests were performed to further understand the charge transfer and ion diffusion processes. Fig. 6(a-d) display a family of Nyquist plots measured from the WO_3 thin films applied by different potentials in the Li^+-based electrolyte with (a-b) and without (c-d) acetic acid in the frequency region ranging from 100 mHz to 100 kHz. The slope in the lower frequency region is decreased when the WO_3 thin films are applied a higher positive voltage, indicating that the ion insertion rate is

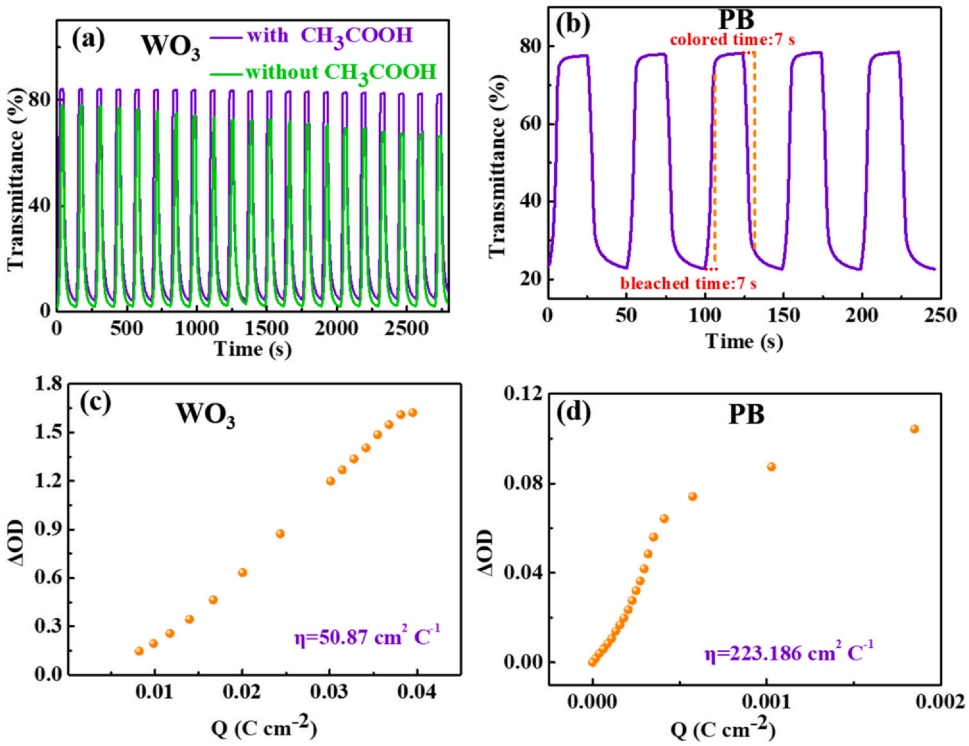

Fig. 5. (a) The time-dependent optical transmittance spectra at $\lambda_{633\,nm}$ (−1.0 V/+1.0 V, 135 s per cycle) for the WO_3 thin films in PC-$LiClO_4$ electrolyte with and without acetic acid. (b) The time-dependent optical transmittance spectra at $\lambda_{633\,nm}$ (−1.0 V/+1.0 V, 100 s per cycles) for the PB films in PC-$LiClO_4$ electrolyte with acetic acid. Plots of the time-dependent optical density variation as a function of charge density at $\lambda_{633\,nm}$ for (c) the WO_3 thin films and (d) the PB films in PC-$LiClO_4$ electrolyte with acetic acid.

reduced gradually [52]. In Fig. 6(b) and 6(d), the Nyquist plots of all the samples show almost similar patterns. It's worth noting that the slopes are near 45° in the low frequency region, matching with the low diffusion resistance character of the WO_3 with highly porous morphology [53]. A simple Randle's equivalent circuit model to evaluate the EIS spectra is shown in the inset of Fig. 6(a) [54]. In the high frequency region, the intercept of the real axis, the diameter of the semicircle in the high-frequency region and *W* represents the resistance (R_s) of the electrolyte, the interfacial charge-transfer resistance (R_{ct}) and the semi-infinite Warburg element, respectively [26,55]. The fitted results (Table S1) manifest that R_s of the WO_3 thin films is estimated to be about 9 Ω cm^{-2} and 13 Ω cm^{-2} in the Li^+-based electrolyte with and without acetic acid, respectively, double confirming that the Li^+&H^+ electrolyte system shows a high ionic conductivity. Moreover, the interfacial charge-transfer resistance in the Li^+&H^+ system is less than that in the Li^+ system at the same applied voltage (Table 1). The R_{ct} is increased obviously with the increase of the negative bias voltage due to the conductor (M_xWO_3)-to-semiconductor (WO_3) transition [14]. Besides, no significant increase of R_{ct} is observed with increasing the positive bias voltage, suggesting that the kinetics to govern the coloring process is slow for the WO_3 thin films. In the inset of Fig. 6(d), the slope of the Nyquist plot is larger than 1, which indicates that the formation of an electrical double layer at the WO_3/electrolyte interface (@ an applied potential of +1.0 V) [56]. Electrochemical impedance spectra of the colored and bleached PB films applied by different potentials in the Li^+-based electrolyte with acetic acid in the frequency region ranging from 100 mHz to 100 kHz are shown in Fig. 6(e-f). The Nyquist plots were modeled with a Randle's equivalent circuit, as shown in the inset of Fig. 6(f). The impedance behaviors of pseudocapacitors are observed from the Nyquist spectra [45,57]. The absolute value of the imagine resistance at the low frequency, as a reciprocal function of the intercalation / extraction capacity [58,59], is quite small at +0.7~+1.0 V as well as at −0.8 V, indicating that the extraction and intercalation of the ions is prominent in these cases. As revealed in Table S2, significant decrease of R_{ct} at +0.7~+1.0 V and −0.8 V is observed, meaning that the PB films at these potentials have a higher film conductivity [60]. The high conductivity is one of the significant factors to give rise to faster reduction/oxidation behaviors and shorter colored/bleached response time [61]. These results are beneficial to the excellent electrochromic performance of the complementary devices prepared.

3.5. Long-term operation mechanism of the WO_3-PB complementary devices

The long-term operation mechanism of the WO_3-PB complementary ECD is explained as follows. When an electric potential is applied between the two ITO electrodes, mobile lithium ions (Li^+) and protons (H^+) will move towards the oppositely charged electrodes to form the WO_3/electrolyte and electrolyte/PB active interfaces, as shown in Fig. 7. At the two active interfaces, the optical modulation is believed to be associated with the double intercalation / extraction of electrons and cations, as the following reversible reactions:

$$WO_3(\text{transparent}) + xe^- + xM \leftrightarrow M_XWO_3(\text{blue}),$$
$$M_4Fe(II)_4[Fe(II)(CN)_6]_3(\text{transparent})$$
$$\leftrightarrow Fe(III)_4[Fe(II)(CN)_6]_3(\text{blue}) + 4e^- + 4M$$
$$(M = H^+\&Li^+). \quad (3)$$

During the reaction processes, the degradation of WO_3 films is inhibited by adding acetic acid in Li^+ electrolyte. On the other hand, the protective effects of acetic acid against the formation of $Fe(OH)_2$ / $Fe(OH)_3$ imply that H^+ may synergistically work with Li^+ on PB electrode. In addition, the improved electrochromic cyclic stability of the WO_3-PB complementary ECD is mostly ascribed to several merits such as a larger

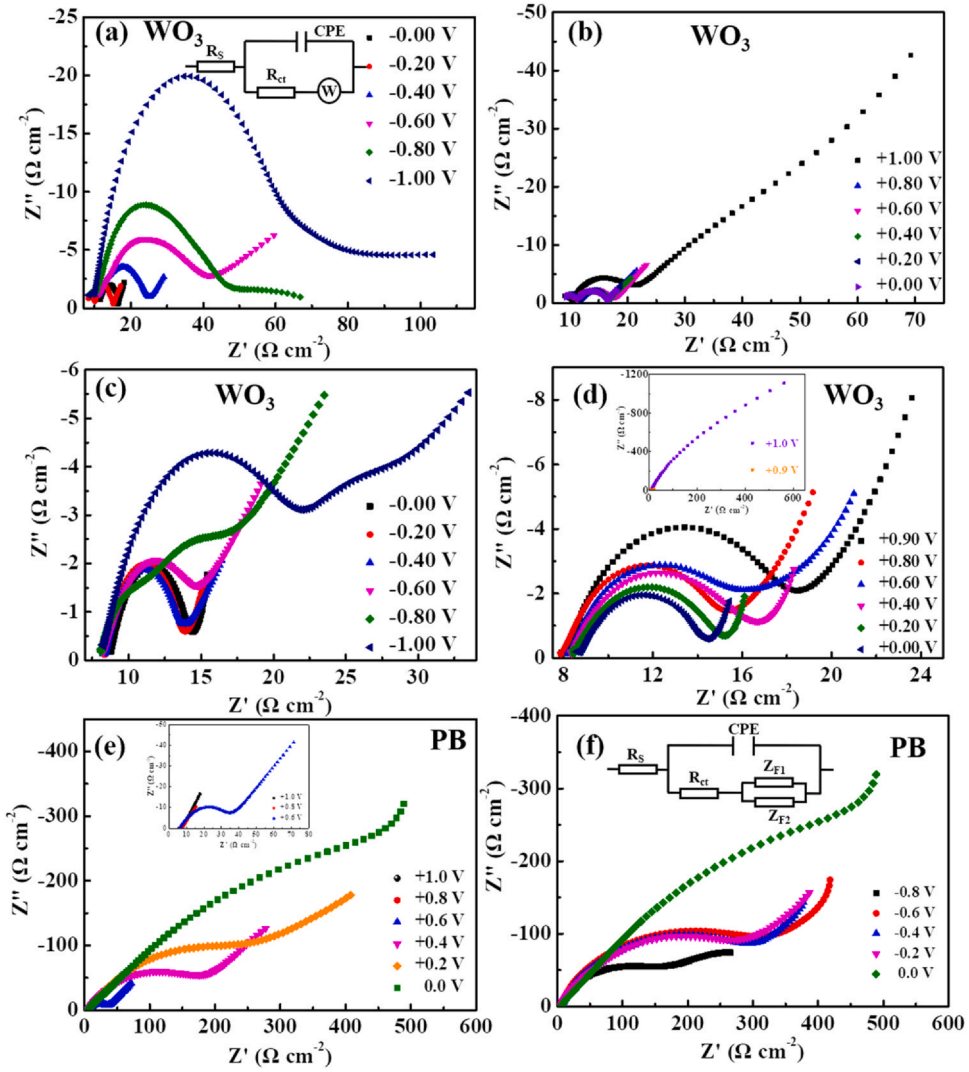

Fig. 6. Nyquist plots measured for the WO_3 thin films in PC-$LiClO_4$ electrolyte with acetic acid at various (a) negative and (b) positive potentials. Nyquist plots measured for the WO_3 thin films in PC-$LiClO_4$ electrolyte without acetic acid at various (c) negative and (d) positive potentials. Nyquist plots measured for the PB films in PC-$LiClO_4$ electrolyte with acetic acid at various (e) positive and (f) negative potentials.

Table 1
Comparison of electrochromic performance between this work and other reported works.

Electrochromic device	Driving potential (V)	Cyclic stability (cycles)	Optical Contrast retention (after cycle)	Capacitance retention (after cycle)	Ref
ITO/PTMA-*co*-BP/electrolyte/ECP-magenta/ITO	−1.35 ~+ 1.2	1800	88.8%	–	[65]
FTO/WO_3/PVA/ PANI/FTO	0 ~+ 1	2500	74.6%	81.4%	[66]
PE/Au/H_2SO_4-doped PANI/ P(VDF-HFP)/ H_2SO_4-doped PANI/Au/PE	−0.05 ~+ 0.3	100	–	–	[67]
FTO/NiO/PB/ electrolyte/WO_3/FTO	−2.3 ~+ 1.3	4000	84.1%	91.4%	[27]
FTO/MnO_2/electrolyte/Mo-doped WO_3/FTO	−1 ~+ 1	2000	–	93.8%	[68]
FTO/WO_3/electrolyte/ rGo/ NiO/FTO	−2.55 ~+ 2.55	2500	–	86.7%	[69]
PET/ITO/P_3HT/gel electrolyte/WO_3/ITO/PET	0 ~+ 1.8	6000	–	95.6%	[26]
ITO/PBV/solid electrolyte/wPB/ITO	−1.0 ~+ 1.7	1000	94%	–	[70]
ITO/WO_3/electrolyte/PB/ITO	−1.5 ~+ 1.6	10,000	79.8%	102.62%	This work

charge capacity, a high optical modulation, a shorter colored/bleached response time by introducing acetic acid into the electrolyte. Besides, there are probably two reasons why the cyclic retention is more than 100% during whole 10,000 continuous cycles. On one hand, a possible explanation is a continuous activation in the active interface, as reported previously [62]. On the other hand, nanocrystal-in-glass structure of the WO_3 films can restrain efficiently the volume change of films during redox process [63], which is beneficial to enhance retention life of devices [64]. To present aforementioned long-term-stable performance of the proposed ECD, a comparison between the proposed ECD in this report and some other reported ECDs was made and summarized, as shown in Table 1, exhibiting that the long-term cyclicity and electrochromic performance in this study are competitive among the literatures.

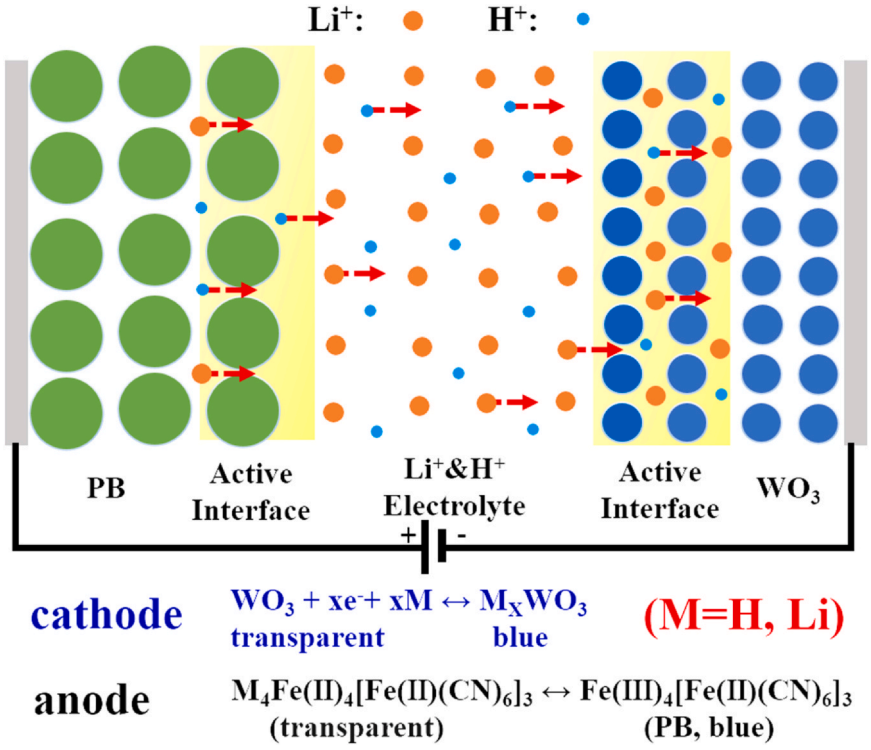

Fig. 7. A schematic diagram of synergistic effects of Li^+ and H^+ on WO_3 and PB electrodes for the WO_3-PB complementary ECD.

4. Conclusion

In summary, the electron beam evaporated nanocrystal-in-glass WO_3 cathodes and the electrochemically deposited hierarchical PB anodes in the Li^+-based electrolyte with or without acetic acid are used to investigate the electrochromic and electrochemical properties. Our findings confirm long-term stability of WO_3 and PB electrodes in the Li^+-based electrolyte with acetic acid, in which both WO_3 and PB also show many advantages such as well-performed charge capacity, optical modulation, colored/bleached response time. Revealing synergistic effects of Li^+ and H^+ at active interfaces of WO_3/electrolyte and electrolyte/PB allows us to fabricate high performance WO_3-PB complementary electrochromic devices with a superior long-term cyclic stability (over 10,000 cycles), a high coloration efficiency (137.80 cm^2 C^{-1}), and a maximum transmittance modulation of 66.22%@633 nm. These results demonstrate that the long-term-stable WO_3-PB complementary ECDs are promising for practical applications.

CRediT authorship contribution statement

Wang kun: Conceptualization, Methodology, Software. **Hongliang Zhang**: Data curation, Writing - original draft. **Guoxin Chen**: Visualization, Formal analysis. **Tian Tian**: Supervision. **Ajay Kumar**: Software, Validation. **Kai Tao**: Investigation. **Lingyan Liang**: Project administration. **Junhua Gao**: Resources. **Hongtao Cao**: Writing - review & editing.

Declaration of Competing Interest

The authors declare that they have no known competing financial interests or personal relationships that could have appeared to influence the work reported in this paper.

Acknowledgements

This project is supported by the National Natural Science Foundation of China (61974148).

Appendix A. Supporting information

Supplementary data associated with this article can be found in the online version at doi:10.1016/j.jallcom.2020.158534.

References

[1] Y. Huang, M.S. Zhu, Y. Huang, Z.X. Pei, H.F. Li, Z.F. Wang, Q. Xue, C.Y. Zhi, Multifunctional energy storage and conversion devices, Adv. Mater. 28 (2016) 8344–8364.
[2] R.J. Mortimer, Electrochromic materials, Chem. Soc. Rev. 26 (1997) 147–156.
[3] G.A. Niklasson, C.G. Granqvist, Electrochromics for smart windows: thin films of tungsten oxide and nickel oxide, and devices based on these, J. Mater. Chem. 17 (2007) 127–156.
[4] R.J. Mortimer, A.L. Dyer, J.R. Reynolds, Electrochromic organic and polymeric materials for display applications, Displays 27 (2006) 2–18.
[5] P. Bonhote, E. Gogniat, F. Campus, L. Walder, M. Gratzel, Nanocrystalline electrochromic displays, Displays 20 (1999) 137–144.
[6] D.R. Rosseinsky, R.J. Mortimer, Electrochromic systems and the prospects for devices, Adv. Mater. 13 (2001) 783–793.
[7] K.-C. Chen, C.-Y. Hsu, C.-W. Hu, K.-C. Ho, A complementary electrochromic device based on Prussian blue and poly(ProDOT-Et2) with high contrast and high coloration efficiency, Sol. Energy Mater. Sol. Cells 95 (2011) 2238–2245.
[8] C.-F. Lin, C.-Y. Hsu, H.-C. Lo, C.-L. Lin, L.-C. Chen, K.-C. Ho, A complementary electrochromic system based on a Prussian blue thin film and a heptyl viologen solution, Sol. Energy Mater. Sol. Cells 95 (2011) 3074–3080.
[9] M.A. Habib, S.P. Maheswari, M.K. Carpenter, A tungsten-trioxide prussian blue complementary electrochromic cell with a polymer electrolyte, J. Appl. Electrochem. 21 (1991) 203–207.
[10] Y. Yue, H. Li, K. Li, J. Wang, H. Wang, Q. Zhang, Y. Li, P. Chen, High-performance complementary electrochromic device based on WO 3·0.33H_2O/PEDOT and prussian blue electrodes, J. Phys. Chem. Solids 110 (2017) 284–289.
[11] D. Weng, M. Li, J. Zheng, C. Xu, High-performance complementary electrochromic device based on surface-confined tungsten oxide and solution-phase N-methyl-phenothiazine with full spectrum absorption, J. Mater. Sci. 52 (2016) 86–95.

[12] G. Cai, M. Cui, V. Kumar, P. Darmawan, J. Wang, X. Wang, A. Lee-Sie, Eh, K. Qian, P.S. Lee, Ultra-large optical modulation of electrochromic porous WO_3 film and the local monitoring of redox activity, Chem. Sci. 7 (2016) 1373–1382.

[13] Z. Wang, X.Y. Wang, S. Cong, F.X. Geng, Z.G. Zhao, Fusing electrochromic technology with other advanced technologies: a new roadmap for future development, Mater. Sci. Eng. R Rep. 140 (2020) 100524.

[14] Z. Jiao, J. Wang, L. Ke, X. Liu, H.V. Demir, M.F. Yang, X.W. Sun, Electrochromic properties of nanostructured tungsten trioxide (hydrate) films and their applications in a complementary electrochromic device, Electrochim. Acta 63 (2012) 153–160.

[15] B.J. Liu, J. Zheng, J.L. Wang, J. Xu, H.H. Li, S.H. Yu, Ultrathin W18O49 nanowire assemblies for electrochromic devices, Nano Lett. 13 (2013) 3589–3593.

[16] K.-C. Cheng, F.-R. Chen, J.-J. Kai, Electrochromic property of nano-composite Prussian Blue based thin film, Electrochim. Acta 52 (2007) 3330–3335.

[17] D. Evecan, E. Zayim, Highly uniform electrochromic tungsten oxide thin films deposited by e-beam evaporation for energy saving systems, Curr. Appl. Phys. 19 (2019) 198–203.

[18] H.-H. Lu, Effects of oxygen contents on the electrochromic properties of tungsten oxide films prepared by reactive magnetron sputtering, J. Alloy. Compd. 465 (2008) 429–435.

[19] S.S. Kalagi, S.S. Mali, D.S. Dalavi, A.I. Inamdar, H. Im, P.S. Patil, Transmission attenuation and chromic contrast characterization of R.F. sputtered WO_3 thin films for electrochromic device applications, Electrochim. Acta 85 (2012) 501–508.

[20] S. Hashimoto, H. Matsuoka, H. Kagechika, M. Susa, K.S. Goto, Degradation of electrochromic amorphous WO_3 film in lithium-salt electrolyte, J. Electrochem. Soc. 137 (1990) 1300–1304.

[21] D. Qiu, H. Ji, X.L. Zhang, H.L. Zhang, H.T. Cao, G.X. Chen, T. Tian, Z.Y. Chen, X. Guo, L.Y. Liang, J.H. Gao, Z.G. Fei, Electrochromism of nanocrystal-in-glass tungsten oxide thin films under various conduction cations, Inorg. Chem. 58 (2019) 2089–2098.

[22] S.J. Babinec, A quartz crystal microbalance analysis of ion insertion into WO_3, Sol. Energy Mater. Sol. Cells 25 (1992) 269–291.

[23] J.P. Randin, Chemical and electrochemical stability of WO_3 electrochromic films in liquid electrolytes, J. Electron. Mater. 7 (1978) 47–63.

[24] J. Li, J.D. Qiu, J.J. Xu, H.Y. Chen, X.H. Xia, The synergistic effect of Prussian-Blue-grafted carbon nanotube/poly(4-vinylpyridine) composites for amperometric sensing, Adv. Funct. Mater. 17 (2007) 1574–1580.

[25] V.B. Isfahani, N. Memarian, H.R. Dizaji, A. Arab, M.M. Silva, The physical and electrochromic properties of Prussian Blue thin films electrodeposited on ITO electrodes, Electrochim. Acta 304 (2019) 282–291.

[26] K.R. Li, Y.L. Shao, S.Y. Liu, Q.H. Zhang, H.Z. Wang, Y.G. Li, R.B. Kaner, Aluminum-ion-intercalation supercapacitors with ultrahigh areal capacitance and highly enhanced cycling stability: power supply for flexible electrochromic devices, Small 13 (2017) 1700380.

[27] J.B. Pan, R.Z. Zheng, Y. Wang, X.K. Ye, Z.Q. Wan, C.Y. Jia, X.L. Weng, J.L. Xie, L.J. Deng, A high-performance electrochromic device assembled with hexagonal WO_3 and NiO/PB composite nanosheet electrodes towards energy storage smart window, Sol. Energy Mater. Sol. Cells 207 (2020) 110337.

[28] Z.T. Li, Y.H. Tang, K.L. Zhou, H. Wang, H. Yan, Effects of pumice-based porous material on hydration characteristics and persistent shrinkage of ultra-high performance concrete (UHPC), Materials 12 (2019) 11.

[29] C. Xu, C. Ma, X. Kong, M. Taya, Vacuum filling process for electrolyte in enhancing electrochromic polymer window assembly, Polym. Adv. Technol. 20 (2009) 178–182.

[30] E. Eren, C. Alver, G.Y. Karaca, E. Uygun, L. Oksuz, A.U. Oksuz, High-performance flexible complementary electrochromic device based on plasma modified WO_3 nano hybrids and V_2O_5 nanofilm with low operation voltages, Electroanal 30 (2018) 2099–2109.

[31] L.Y. Zhang, S.X. Xiong, J. Ma, X.H. Lu, A complementary electrochromic device based on polyaniline-tethered polyhedral oligomeric silsesquioxane and tungsten oxide, Sol. Energy Mater. Sol. Cells 93 (2009) 625–629.

[32] H.Y. Qu, H.C. Zhang, N. Li, Z.Q. Tong, J. Wang, J.P. Zhao, Y. Li, A rapid-response electrochromic device with significantly enhanced electrochromic performance, RSC Adv. 5 (2015) 803–806.

[33] J. Bae, D.G. Seo, S.M. Park, K.T. Park, H. Kim, H.C. Moon, S.H. Kim, Optimized low-temperature fabrication of WO_3 films for electrochromic devices, J. Phys. D Appl. Phys. 50 (2017) 465105.

[34] Y. Chen, Z. Bi, X. Li, X. Xu, S. Zhang, X. Hu, High-coloration efficiency electrochromic device based on novel porous TiO_2@prussian blue core-shell nanostructures, Electrochim. Acta 224 (2017) 534–540.

[35] S.H. Lee, R. Deshpande, P.A. Parilla, K.M. Jones, B. To, A.H. Mahan, A.C. Dillon, Crystalline WO_3 nanoparticles for highly improved electrochromic applications, Adv. Mater. 18 (2006) 763–766.

[36] M. Guzel, E. Karatas, M. Ak, Synthesis and fluorescence properties of carbazole based asymmetric functionalized star shaped polymer, J. Electrochem. Soc. 164 (2017) H49–H55.

[37] S.S. Zhou, C. Hao, J.J. Wang, X.H. Wang, H.W. Gao, Metal-organic framework templated synthesis of porous NiCo2O4/ZnCo2O4/CO3O4 hollow polyhedral nanocages and their enhanced pseudocapacitive properties, Chem. Eng. J. 351 (2018) 74–84.

[38] Y. Yang, S. Li, F. Liu, J. Wen, N. Zhang, S. Wang, K. Liu, Enhanced performance of multi-dimensional CoS nanoflake/NiO nanosheet architecture with synergetic effect for asymmetric supercapacitor, Nanotechnology 29 (2018) 455401.

[39] J.J. Guo, M. Wang, X.G. Diao, Z.B. Zhang, G.B. Dong, H. Yu, F.M. Liu, H. Wang, J. Liu, Prominent electrochromism achieved using aluminum ion insertion/extraction in amorphous WO_3 films, J. Phys. Chem. C 122 (2018) 19037–19043.

[40] Z.H. Jiao, X.W. Sun, J.M. Wang, L. Ke, H.V. Demir, Hydrothermally grown nanostructured WO_3 films and their electrochromic characteristics, J. Phys. D Appl. Phys. 43 (2010) 285501.

[41] R. Li, K. Li, G. Wang, L. Li, Q. Zhang, J. Yan, Y. Chen, Q. Zhang, C. Hou, Y. Li, H. Wang, Ion-transport design for high-performance Na(+)-based electrochromics, ACS Nano 12 (2018) 3759–3768.

[42] J. Wang, J. Polleux, J. Lim, B. Dunn, Pseudocapacitive contributions to electrochemical energy storage in TiO_2 (anatase) nanoparticles, J. Phys. Chem. C 111 (2007) 14925–14931.

[43] J.B. Mitchell, W.C. Lo, A. Genc, J. LeBeau, V. Augustyn, Transition from battery to pseudocapacitor behavior via structural water in tungsten oxide, Chem. Mater. 29 (2017) 3928–3937.

[44] L.C. Chen, K.C. Ho, Nonlinear diffusion Behavior for the Prussian blue electrode - II. Interpretation of variable diffusivity during the insertion/extraction processes, J. Electrochem. Soc. 149 (2002) E40–E44.

[45] M.J. Qiu, P. Sun, L.X. Shen, K. Wang, S.Q. Song, X. Yu, S.Z. Tan, C.X. Zhao, W.J. Mai, WO_3 nanoflowers with excellent pseudo-capacitive performance and the capacitance contribution analysis, J. Mater. Chem. A 4 (2016) 7266–7273.

[46] C. Bohnke, O. Bohnke, Impedance analysis of amorphous wo3 thin-films in hydrated liclo4-propylene carbonate electrolytes, Solid State Ion. 39 (1990) 195–204.

[47] N. Yoshiike, Y. Mizuno, S. Kondo, Behavior of the evaporated WO_3 film in li-salt pc electrolytes, J. Electrochem. Soc. 131 (1984) 2634–2641.

[48] H.J. Ahn, H.S. Shim, Y.E. Sung, T.Y. Seong, W.B. Kim, Electrochromism of Sn-modified WO_3 electrodes prepared from sol-gel method, Electrochem. Solid State Lett. 10 (2007) E27–E30.

[49] R. Giannuzzi, R. Scarfiello, T. Sibillano, C. Nobile, V. Grillo, C. Giannini, P.D. Cozzoli, M. Manca, From capacitance-controlled to diffusion-controlled electrochromism in one-dimensional shape-tailored tungsten oxide nanocrystals, Nano Energy 41 (2017) 634–645.

[50] C.Z. Hua, G.Z. Yuan, Z.Q. Cheng, H. Jiang, G. Xu, Y. Liu, G.R. Han, Building architecture of TiO_2 nanocrystals embedded in amorphous WO3 films with improved electrochromic properties, Electrochim. Acta 309 (2019) 354–361.

[51] C.L. Lin, L.C. Liao, Preparation and characterization of micropatterned prussian blue thin films with enhanced electrochromic properties, Surf. Coat. Tech. 259 (2014) 330–334.

[52] Y. Wang, R.Z. Zheng, J.S. Luo, H.A. Malik, Z.Q. Wan, C.Y. Jia, X.L. Weng, J.L. Xie, L.J. Deng, X.J. Yao, Self-healing dynamically cross linked versatile polymer electrolyte: a novel approach towards high performance, flexible electrochromic devices, Electrochim. Acta 320 (2019) 134489.

[53] S.K. Meher, P. Justin, G.R. Rao, Nanoscale morphology dependent pseudocapacitance of NiO: influence of intercalating anions during synthesis, Nanoscale 3 (2011) 683–692.

[54] P.T.G. Gayathri, S. Sajitha, I. Vijitha, S.S. Shaiju, R. Remya, B. Deb, Tuning of physical and electrochemical properties of nanocrystalline tungsten oxide through ultraviolet photoactivation, Electrochim. Acta 272 (2018) 135–143.

[55] M. Jamdegni, A. Kaur, Electrochromic behavior of highly stable, flexible electrochromic electrode based on covalently bonded polyaniline-graphene quantum dot composite, J. Electrochem. Soc. 166 (2019) H502–H509.

[56] N. Ogihara, S. Kawauchi, C. Okuda, Y. Itou, Y. Takeuchi, Y. Ukyo, Theoretical and experimental analysis of porous electrodes for lithium-ion batteries by electrochemical impedance spectroscopy using a symmetric cell, J. Electrochem. Soc. 159 (2012) A1034–A1039.

[57] M. Zhu, W. Meng, Y. Huang, Y. Huang, C. Zhi, Proton-insertion-enhanced pseudocapacitance based on the assembly structure of tungsten oxide, ACS Appl. Mater. Interfaces 6 (2014) 18901–18910.

[58] M.D. Levi, D. Aurbach, Diffusion coefficients of lithium ions during intercalation into graphite derived from the simultaneous measurements and modeling of electrochemical impedance and potentiostatic intermittent titration characteristics of thin graphite electrodes, J. Phys. Chem. B 101 (1997) 4641–4647.

[59] F. Nobili, R. Tossici, R. Marassi, F. Croce, B. Scrosati, An AC impedance spectroscopic study of $LixCoO_2$ at different temperatures, J. Phys. Chem. B 106 (2002) 3909–3915.

[60] J.J. Garciajareno, J.J. Navarro, A.F. Roig, H. Scholl, F. Vicente, Impedance analysis of prussian-blue films deposited on ito electrodes, Electrochim. Acta 40 (1995) 1113–1119.

[61] G.K. Pande, J.H. Choi, J.E. Lee, Y.E. Kim, J.H. Choi, H.W. Choi, H.G. Chae, J.S. Park, Octa-viologen substituted polyhedral oligomeric silsesquioxane exhibiting outstanding electrochromic performances, Chem. Eng. J. 393 (2020) 124690.

[62] H. Chen, M. Zhou, Z. Wang, S.Y. Zhao, S.Y. Guan, Rich nitrogen-doped ordered mesoporous phenolic resin-based carbon for supercapacitors, Electrochim. Acta 148 (2014) 187–194.

[63] W. Kaveevivitchai, A. Huq, S. Wang, M.J. Park, A. Manthiram, Rechargeable aluminum-ion batteries based on an open-tunnel framework, Small 13 (2017) 1701296.

[64] H.L. Wang, Q.L. Hao, X.J. Yang, L.D. Lu, X. Wang, A nanostructured graphene/polyaniline hybrid material for supercapacitors, Nanoscale 2 (2010) 2164–2170.

[65] J. He, S. Mukherjee, X. Zhu, L. You, B.W. Boudouris, J. Mei, Highly transparent crosslinkable radical copolymer thin film as the ion storage layer in organic electrochromic devices, ACS Appl. Mater. Interfaces 10 (2018) 18956–18963.

[66] W.Q. Wang, X.L. Wang, X.H. Xia, Z.J. Yao, Y. Zhong, J.P. Tu, Enhanced electrochromic and energy storage performance in mesoporous WO_3 film and its application in a bi-functional smart window, Nanoscale 10 (2018) 8162–8169.

[67] G. Xu, L. Zhang, B. Wang, X. Chen, S. Dou, M. Pan, F. Ren, X. Li, Y. Li, A visible-to-infrared broadband flexible electrochromic device based polyaniline for simultaneously variable optical and thermal management, Sol. Energy Mater. Sol. Cells 208 (2020) 110356.
[68] S. Xie, Y. Chen, Z. Bi, S. Jia, X. Guo, X. Gao, X. Li, Energy storage smart window with transparent-to-dark electrochromic behavior and improved pseudocapacitive performance, Chem. Eng. J. 370 (2019) 1459–1466.
[69] X. Xia, Z. Ku, D. Zhou, Y. Zhong, Y. Zhang, Y. Wang, M.J. Huang, J. Tu, H.J. Fan, Perovskite solar cell powered electrochromic batteries for smart windows, Mater. Horiz. 3 (2016) 588–595.
[70] M.S. Fan, S.Y. Kao, T.H. Chang, R. Vittal, K.C. Ho, A high contrast solid-state electrochromic device based on nano-structural Prussian blue and poly(butyl viologen) thin films, Sol. Energy Mater. Sol. Cells 145 (2016) 35–41.